

Dynamical preparation of EPR entanglement in two-well Bose-Einstein condensates

B. Opanchuk¹, Q. Y. He^{1,2}, M. D. Reid^{1,*}, and P. D. Drummond^{1,†}

¹*Centre for Atom Optics and Ultrafast Spectroscopy,*

Swinburne University of Technology, Melbourne 3122, Australia

²*State Key Laboratory of Mesoscopic Physics, School of Physics,
Peking University, Beijing 100871, People's Republic of China and*

[†]*pdrummond@swin.edu.au, *mdreid@swin.edu.au*

We propose to generate Einstein-Podolsky-Rosen (EPR) entanglement between groups of atoms in a two-well Bose-Einstein condensate using a dynamical process similar to that employed in quantum optics. The local nonlinear S -wave scattering interaction has the effect of creating a spin squeezing at each well, while the tunneling, analogous to a beam splitter in optics, introduces an interference between these fields that results in an inter-well entanglement. We consider two internal modes at each well, so that the entanglement can be detected by measuring a reduction in the variances of the sums of local Schwinger spin observables. As is typical of continuous variable (CV) entanglement, the entanglement is predicted to increase with atom number, and becomes sufficiently strong at higher numbers of atoms that the EPR paradox and steering non-locality can be realized. The entanglement is predicted using an analytical approach and, for larger atom numbers, stochastic simulations based on truncated Wigner function. We find generally that strong tunnelling is favourable, and that entanglement persists and is even enhanced in the presence of realistic nonlinear losses.

I. INTRODUCTION

Entanglement between groups of atoms has been confirmed experimentally, and recent experiments report the development of quantum correlated twin-atom beams [1–4]. This represents a first benchmark for investigations into multi-particle non-locality that could deepen our understanding of the “classicality versus quantumness” for macroscopic objects [5]. So far, however, there has been no reported conclusive demonstration of stronger forms of quantum non-locality (such as violations of Bell inequalities [6], the Einstein-Podolsky-Rosen paradox [7–9] or steering [10–12]) using mesoscopic groups of atoms, although there have been a number of theoretical proposals and studies of the correlation between spatially separated atoms [13–20]. Highly efficient detection of an Einstein-Podolsky-Rosen (EPR) paradox for quadrature field amplitudes [8, 9], and loophole-free steering for photons [12], has been been realized in optics.

In this paper, our goal is to develop a strategy for generating spatial entanglement between mesoscopic groups of atoms confined to the potential wells of an ultra-cold Bose Einstein condensate (BEC). Such atoms have been verified entangled [21], but we seek to achieve an unambiguous EPR paradox-steering type of entanglement, in which the entanglement between the atoms of different wells can be characterized, and readily extended to situations involving the genuine multi-partite entanglement of groups of atoms at three or more sites [22]. Apart from the potential to test quantum mechanics in new regimes, this type of entanglement underpins many important applications in the fields of quantum information and metrology [23–26].

There are many possible strategies for the generation of such spatial multi-atom EPR entanglement. A recent experiment demonstrates EPR-type correlation near the coherent noise level using spin changing collisions

[3], and there has been a recent proposal to create spatial entanglement between two wells by direct adiabatic cooling to the ground state [27]. The most common method used in quantum optics however is to combine two squeezed single mode fields through a beam splitter (BS) [9, 26, 28, 29]. The method relies on a nonlinearity to produce squeezing in each mode locally, followed by a linear coupling transformation to create the entanglement between the two modes.

Motivated by this, we explore in this paper a similar dynamical strategy applied to the BEC double potential well system. Following Milburn et al [30], we assume the atoms of each well can be modeled using a single mode approximation, and introduce the respective boson operators, a and b . In this case, the S -wave scattering intra-well interactions, given by Hamiltonians $\hat{H} = \hbar g \hat{a}^{\dagger 2} \hat{a}^2$ and $\hat{H} = \hbar g \hat{b}^{\dagger 2} \hat{b}^2$, provide the nonlinearity at each well that generates a local spin squeezing, while the coupling or tunneling inter-well term, modeled as $\hat{H} = \hbar \kappa (\hat{a}^{\dagger} \hat{b} + \hat{a} \hat{b}^{\dagger})$, provides the linear beam-splitter transformation [31, 32] that generates inter-well two-mode entanglement.

We consider in fact two dynamical strategies: in the first the local nonlinear and nonlocal tunnelling processes act sequentially; in the second they act simultaneously. While the second strategy is likely to be more practical, we analyze the sequential case first, in the earlier sections of the paper, because it allows a full quantum solution within the constraints of the two-mode model.

We show that substantial entanglement can be generated in both cases, provided parameters are optimized. An analysis of what is accessible experimentally indicates that this entanglement could be within reach of current set-ups, though the realization of EPR and steering paradoxes presents a greater challenge, and may require more sophisticated experimental procedures.

Perhaps surprisingly, we find that a large amount of en-

tanglement requires using large numbers of atoms. This result is verified using both a full quantum analysis and the truncated Wigner function [33] which becomes valid as $1/N^{3/2} \rightarrow 0$. The manifestation of a continuous variable (CV) EPR paradox has been shown for large optical amplitudes [34], but may have been thought impossible to realize for large groups of atoms. The prediction is consistent with those of Ferris et al [19] and who study EPR entanglement in BEC four wave mixing, though in our case an atomic homodyne detection [3] is not used, the EPR observables being the local Schwinger spins that can be measured via Rabi rotation and atom counting.

The paper is organized as follows. We first summarize in Section II the meaning of Einstein-Podolsky-Rosen entanglement, and outline how it is to be detected. The dynamical solutions for the entanglement via the two-step method are presented in Sections III and IV. The truncated Wigner function simulations and the results for the inter-well entanglement via simultaneous evolution are treated in Section V. An analysis modeling current experimental regimes, including the effect of nonlinear losses, indicates that the EPR entanglement is robust against the expected decoherence effects.

II. EPR ENTANGLEMENT

The original CV EPR paradox [7] considers correlations between the positions and momenta of two particles emitted from a source. With optical or atomic Bose fields, one can define the quadrature phase amplitudes of two spatially separated field modes, as $\hat{X}_A = (\hat{a}^\dagger + \hat{a})/2$, and $\hat{P}_A = (\hat{a}^\dagger - \hat{a})/2i$, and $\hat{X}_B = (\hat{b}^\dagger + \hat{b})/2$, and $\hat{P}_B = (\hat{b}^\dagger - \hat{b})/2i$. These are analogous to the position and momentum in the two-particle system.

The EPR paradox arises when both \hat{X}_A and \hat{X}_B , and \hat{P}_A and \hat{P}_B , are maximally correlated, so that measurement of \hat{X}_A enables exact prediction of the outcome for measurement of \hat{X}_B , and the measurement of \hat{P}_A enables exact prediction of the outcome of measurement of \hat{P}_B . EPR argued that, assuming no “spooky action at distance”, the action of measuring \hat{X}_A could not “create” the result for \hat{X}_B . They then concluded, since the result for \hat{X}_B can be predicted without disturbance of that system, that the result for the outcome is predetermined. Since the predetermination of both \hat{X}_B and \hat{P}_B is without uncertainty, there can be no equivalent local quantum state interpretation. Hence, EPR argued that quantum mechanics was incomplete. The premises assumed by EPR are often termed “local realism”, and the EPR paradox can be thought of as a demonstration of the incompatibility between “local realism” and the “completeness of quantum mechanics”.

EPR’s argument applies when one observer (Alice) can make precise predictions for the outcome of measurements made by a second, distant observer (Bob). The key issue for the EPR paradox is that Alice can infer a result for either of two of Bob’s conjugate observables,

by measuring locally on her system. The EPR paradox arises when the accuracy of her inferences would violate quantum mechanics, if she could infer results for both conjugate observables simultaneously. This demonstration of the EPR paradox is most simply achieved by comparing the conditional variances for Alice’s measurements with the variances of the Heisenberg uncertainty relation [9, 35].

A. Entanglement criteria

The original EPR paradox focused on states that showed correlation and anti-correlation for position and momentum respectively. Duan et al and Simon [36, 37] showed that entanglement between modes a and b is confirmed if

$$D = \Delta^2(\hat{X}_A - \hat{X}_B) + \Delta^2(\hat{P}_A + \hat{P}_B) < 1. \quad (\text{II.1})$$

In the case (II.1), the 1 arises from the commutation relation $[\hat{a}, \hat{a}^\dagger] = 1$, and reflects the quantum noise associated with the four observables. A more general criterion is the product form: entanglement is confirmed when $\Delta(\hat{X}_A - \hat{X}_B)\Delta(\hat{P}_A + \hat{P}_B) < 1/2$ [29, 38].

Quadrature phase amplitudes are measured using local oscillator methods, in which a strong field interferes with a signal field, using a beam splitter. A full analysis of a local oscillator measurement shows that it is actually equivalent to a Schwinger spin measurement, once the local oscillator is accounted for. It is useful to consider entanglement measures that have been developed for spin measurements. In particular, one can show entanglement using the spin version of (II.1) [29],

$$\Delta^2(\hat{J}_A^X \mp \hat{J}_B^X) + \Delta^2(\hat{J}_A^Y \pm \hat{J}_B^Y) < |\langle \hat{J}_A^Z \rangle| + |\langle \hat{J}_B^Z \rangle|, \quad (\text{II.2})$$

and also the Heisenberg-product entanglement criterion [38]

$$\sqrt{\Delta^2(\hat{J}_A^\theta - \hat{J}_B^\theta) \cdot \Delta^2(\hat{J}_A^{\theta+\pi/2} + \hat{J}_B^{\theta+\pi/2})} < \frac{|\langle \hat{J}_A^Y \rangle| + |\langle \hat{J}_B^Y \rangle|}{2}. \quad (\text{II.3})$$

B. EPR paradox steering criteria

While entanglement as confirmed by (II.1) is necessary for the EPR paradox, it is not sufficient. To quantitatively demonstrate the paradox, in the style constructed by EPR, the level of correlation in Alice’s predictions must be compared with the quantum limit for a local state that might predetermine Bob’s statistics. Thus, for the EPR paradox, the relevant quantum noise level is that of one observer, B , alone.

The EPR paradox confirms “steering”, whereas the entanglement of (II.1) does not. Steering has been established as a distinct form of non-locality [10]. The EPR

paradox and steering types of entanglement provide a distinct resource for quantum information with applications not achievable for arbitrary entangled states [25].

An EPR paradox signature has been formulated in terms of conditional variances [35]: thus EPR entanglement is observed when

$$\Delta(\hat{X}_B|\hat{X}_A)\Delta(\hat{P}_B|\hat{P}_A) < 1/4. \quad (\text{II.4})$$

Since the precise choice of measurement at mode A is not important, only the inference, this criterion is sometimes more generally written as $\Delta_{\text{inf}}\hat{X}_B\Delta_{\text{inf}}\hat{P}_B < 1$.

More recently, it has been pointed out that the EPR signature is achieved once the entanglement variances become small enough [9, 19]. EPR entanglement is detected, if either

$$D = \Delta^2(\hat{X}_A - \hat{X}_B) + \Delta^2(\hat{P}_A + \hat{P}_B) < 1/2, \quad (\text{II.5})$$

or $\Delta(\hat{X}_A - \hat{X}_B)\Delta(\hat{P}_A + \hat{P}_B) < 1/4$. These criteria are special cases of (II.4), and may not give the optimal measurement strategy for obtaining an EPR paradox, but are useful in many practical cases where only (II.5) is measured.

Spin EPR measures can also be obtained, just as with entanglement *per se*, using the inferred Heisenberg uncertainty principle approach. From the Heisenberg spin uncertainty relation $\Delta\hat{J}_B^X\Delta\hat{J}_B^Y \geq |\langle\hat{J}_B^Z\rangle|/2$, one can derive several simple spin-EPR criteria [9, 29, 39]. For the case of a large non-zero mean spin, taken for definiteness in the z -direction, an EPR paradox is demonstrated when

$$\Delta_{\text{inf}}\hat{J}_B^X\Delta_{\text{inf}}\hat{J}_B^Y < \frac{1}{2}|\langle\hat{J}_B^Z\rangle|. \quad (\text{II.6})$$

This criterion for the EPR paradox can be expressed in a particularly useful, though less general form, as follows:

$$\sqrt{\Delta^2(\hat{J}_A^\theta - g\hat{J}_B^\theta) \cdot \Delta^2(\hat{J}_A^{\theta+\pi/2} + g'\hat{J}_B^{\theta+\pi/2})} < \frac{|\langle\hat{J}_B^Y\rangle|}{2}. \quad (\text{II.7})$$

In this version, the simplification has been made that the inference is given using a fixed linear approximation with constant gain g .

III. DYNAMICAL PREPARATION OF BEC EPR ENTANGLEMENT

We now turn to examining how to generate EPR entanglement in a BEC. A two-well BEC system can be modeled by the two-mode Hamiltonian [30]:

$$\hat{H}/\hbar = \kappa(\hat{a}^\dagger\hat{b} + \hat{a}\hat{b}^\dagger) + \frac{g}{2}(\hat{a}^\dagger\hat{a}^\dagger\hat{a}\hat{a} + \hat{b}^\dagger\hat{b}^\dagger\hat{b}\hat{b}). \quad (\text{III.1})$$

Here κ is the conversion rate between the two components, denoted by mode operators a and b , and g is the nonlinear self interaction coefficient proportional to the three-dimensional S-wave scattering length, a_{3D} . The

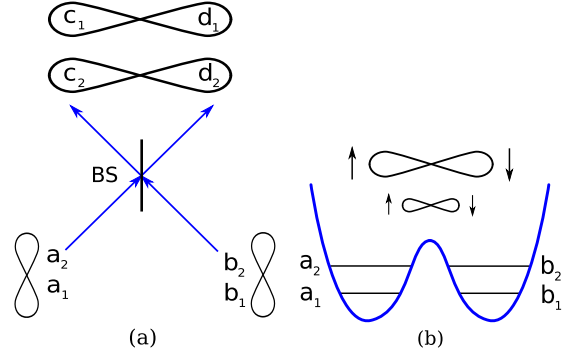


Figure 1. Creation of spatial entanglement between modes a_i and b_i at different sites. The optical scheme is depicted in (a) and the BEC two-well proposal in (b). Local spin squeezing can be produced when the two modes at each well evolve for a time τ under the nonlinear Hamiltonian (IV.1). Depending on the exact configuration, there can be coupling terms between the two modes at each site. The well height is controlled to allow a tunneling cross-interaction between the modes. This is equivalent to the modes interfering using a beam splitter, and the effect is to generate an inter-well spatial entanglement.

first term proportional to κ describes an exchange of particles between the two wells (modes) in which total number is conserved. This linear term is equivalent to that for an optical beam splitter [31, 32]. The Hamiltonian model applies to other two-mode bosonic systems including optical cavity modes or superconducting wave-guides with a nonlinear medium, as well as other types of two-mode atomic systems. However, we will use a two-well picture to illustrate the gedanken-experiment we have in mind, even though implementations may not be exactly in this form. The two-well model and system has been studied extensively in relation to macroscopic superposition states [32, 40] and ultra-sensitive interferometric measurement [41, 42].

If, in addition, we allow two internal spin components per well, the Hamiltonian becomes:

$$\hat{H}/\hbar = \sum_i \kappa_i \hat{a}_i^\dagger \hat{b}_i + \frac{1}{2} \sum_{ij} g_{ij} \hat{a}_i^\dagger \hat{a}_j^\dagger \hat{a}_j \hat{a}_i + \left\{ \hat{a}_i \leftrightarrow \hat{b}_i \right\}. \quad (\text{III.2})$$

Here we consider two internal modes at each EPR site A and B , with four modes in total, as shown schematically in Fig. 1. The local modes can be independent (in which case local cross couplings g_{ij} are zero), or not independent, as where the modes are coupled by the BEC self interaction term [42]. The coupling constant is proportional to the three-dimensional S-wave scattering length, so that $g_{ij} \propto a_{ij}$, as in the two-mode case.

We will describe our results using the equivalent dimensionless Hamiltonian

$$\tilde{H} = \sum_i \tilde{\kappa}_i \hat{a}_i^\dagger \hat{b}_i + \frac{1}{2} \sum_{ij} \tilde{g}_{ij} \hat{a}_i^\dagger \hat{a}_j^\dagger \hat{a}_j \hat{a}_i + \left\{ \hat{a}_i \leftrightarrow \hat{b}_i \right\}, \quad (\text{III.3})$$

with dimensionless coefficients $\tilde{\kappa}_i = \kappa_i/g_{11}N_A$, $\tilde{g}_{ij} =$

$g_{ij}/g_{11}N_A$, where N_A is the initial total boson number in well A, and a corresponding dimensionless time $\tau = g_{11}N_A t$. For definiteness, we will choose ratios of nonlinear couplings \tilde{g}_{ij} to correspond to known S-wave scattering lengths of ^{87}Rb , (between $|1\rangle \equiv |F=1, m_F=+1\rangle$ and $|2\rangle \equiv |F=2, m_F=-1\rangle$) at specific magnetic field strengths near a Feshbach resonance $B = 9.105\text{ G}$. Namely, we use $B = 9.086\text{ G}$ with corresponding $a_{12} = 107.8a_0$, and $B = 9.116\text{ G}$ with corresponding $a_{12} = 80.8a_0$ [43], where a_0 is the Bohr radius. Intra-species scattering length are constant and equal to $a_{11} = 100.4a_0$ and $a_{22} = 95.5a_0$. Other results will be given as well.

We propose to generate EPR states by preparing the system in a multi-mode coherent state and then allowing evolution according to the Hamiltonian (III.1). Two strategies are compared. Firstly, where a manipulation of tunneling (e.g., by changing the potential barrier height) occurs, so that the nonlinear and linear terms are applied sequentially, and secondly, where the nonlinear and linear tunneling terms act simultaneously, as in (III.1–III.3). The second strategy is likely to be more readily implemented, and is solved for in Section V via a truncated Wigner function method, with the inclusion of further effects such as nonlinear losses.

In the two-step strategy, local squeezing is first generated for each mode a and b via the nonlinear Hamiltonian in the absence of tunneling, and subsequently, a strong tunneling interaction provides a linear mixing that generates an EPR entanglement between the two new modes c and d . The strategy is depicted in Fig. 1. The technique is similar to that investigated experimentally in fibre-optics entanglement [44]. An important difference is that the fiber experiment used time-delayed pulses and dispersion to eliminate interactions, that is local cross couplings, between the components. This is not readily feasible in BEC experiments, although Feshbach resonances can achieve this to a limited extent. In the next Section, we present full quantum solutions for this two-step strategy.

We briefly remark on our choice of initial conditions. In experiments with multiple wells, it is generally possible to prepare condensates with relative phase coherence, provided that tunneling is strong enough during the evaporative cooling process. The overall phase is random, with a total number uncertainty that is typically at least Poissonian. This quantum state is therefore well represented by a mixture of coherent states with a random overall phase. However, since none of our results depend on the overall phase, it is sufficient to consider just a single overall coherent state with an arbitrary phase. This is a low-temperature limit, which will develop additional fluctuations as temperatures are increased to the critical temperature.

IV. STRATEGY I: TWO-STEP DYNAMICAL ENTANGLEMENT GENERATION

A. Generation of local spin squeezing

In the first step, squeezing is generated locally via a nonlinearity, given by the Hamiltonian

$$\tilde{\mathcal{H}} = \sum_{i,j} \frac{\tilde{g}_{ij}}{2} \hat{a}_i^\dagger \hat{a}_j^\dagger \hat{a}_j \hat{a}_i. \quad (\text{IV.1})$$

The initial state is a product coherent state for each mode: $|\alpha/\sqrt{2}\rangle_{a_1} |\alpha/\sqrt{2}\rangle_{a_2}$. This models the relative coherence between the wells obtained with a low inter-well potential barrier, together with an overall Poissonian number fluctuation that is typically found in an experimental BEC. We explain in the Appendix how to calculate the nonlinear quantum dynamical solutions of (IV.1). These are exact calculations, provided the original multi-mode Hamiltonian can be reduced to simple one or two-mode forms.

Let \hat{a}_1, \hat{a}_2 be operators for the two internal states at well A, and \hat{b}_1, \hat{b}_2 operators for two internal states at well B. Here $\hat{N}_A = \hat{a}_2^\dagger \hat{a}_2 + \hat{a}_1^\dagger \hat{a}_1$ and $\hat{N}_B = \hat{b}_2^\dagger \hat{b}_2 + \hat{b}_1^\dagger \hat{b}_1$ are the atom number operators of these modes in each well. We introduce a phase-rotated Schwinger spin operator measurement that can be performed at each site. For site A, we define

$$\begin{aligned} \hat{J}_A^X &= \frac{1}{2} \left(\hat{a}_2^\dagger \hat{a}_1 e^{i\Delta\theta} + \hat{a}_1^\dagger \hat{a}_2 e^{-i\Delta\theta} \right), \\ \hat{J}_A^Y &= \frac{1}{2i} \left(\hat{a}_2^\dagger \hat{a}_1 e^{i\Delta\theta} - \hat{a}_1^\dagger \hat{a}_2 e^{-i\Delta\theta} \right), \\ \hat{J}_A^Z &= \frac{1}{2} \left(\hat{a}_2^\dagger \hat{a}_2 - \hat{a}_1^\dagger \hat{a}_1 \right), \end{aligned} \quad (\text{IV.2})$$

where $\Delta\theta = \theta_2 - \theta_1$ is the phase shift between the mode 1 and mode 2. There is also an analogous definition at B with phase shift $\Delta\phi = \phi_2 - \phi_1$.

We select the phase shift to ensure $\langle \hat{J}^Y \rangle \neq 0$, and the Schwinger spin operators orthogonal to \hat{J}^Y are given by

$$\hat{J}^\theta = \cos(\theta) \hat{J}^Z + \sin(\theta) \hat{J}^X \quad (\text{IV.3})$$

all of which have the property $\langle \hat{J}^\theta \rangle = 0$. Here $\Delta\theta = \Delta\phi = \pi/2 - \alpha$, and α is time dependent given by the character of $\langle \hat{a}_2^\dagger \hat{a}_1 \rangle = |\langle \hat{a}_2^\dagger \hat{a}_1 \rangle| e^{i\alpha}$. This plane contains an infinite family of maximally conjugate Schwinger spin operators, generally given by \hat{J}^θ and $\hat{J}^{\theta+\pi/2}$ which obey the Heisenberg uncertainty relation

$$\Delta \hat{J}^\theta \Delta \hat{J}^{\theta+\pi/2} \geq |\langle \hat{J}^Y \rangle|/2. \quad (\text{IV.4})$$

Quantum squeezing occurs when the variance in one conjugate observable is reduced below the Heisenberg limit. Thus,

$$\Delta^2 \hat{J}^\theta < |\langle \hat{J}^Y \rangle|/2 \quad (\text{IV.5})$$

is said to be a “spin squeezed” state [45–47].

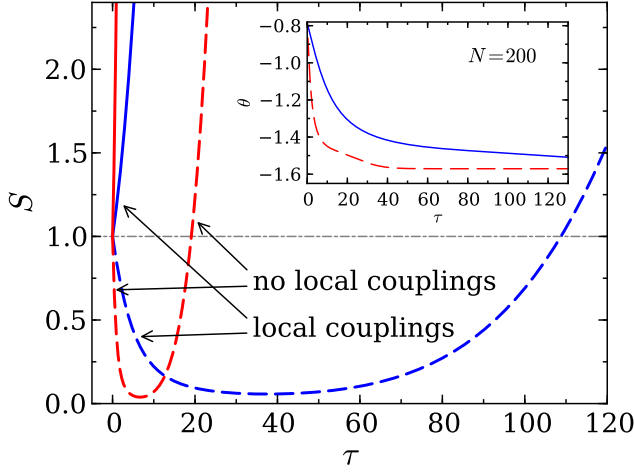


Figure 2. (Color online) Squeezing of local Schwinger spin operators versus interaction time τ . The plot shows the squeezing $\Delta^2 \hat{J}^\theta / n_0$ (solid lines), and $\Delta^2 \hat{J}^{\theta+\pi/2} / n_0$ (dashed lines), where the shot noise level is $n_0 = |\langle \hat{J}^Y \rangle|/2$. Squeezing is obtained when $S = \Delta^2 \hat{J}^{\theta, \theta+\pi/2} / (|\langle \hat{J}^Y \rangle|/2) < 1$. Inset shows the optimal phase choice θ for squeezing. The dimensionless coupling parameters correspond to ^{87}Rb atoms at magnetic field $B = 9.116 \text{ G}$ (blue lines), with corresponding scattering lengths, as explained in the text. We also give results for the case without local cross couplings (red lines), i.e., $g_{12} = 0$, $g_{22} = g_{11}$. Here $N_A = 200$.

Figure 2 shows the prediction for dynamical spin-squeezing, according to the solutions explained in the Appendix A, based on the Hamiltonian Eq. (IV.1). Here we have assumed that a_1, b_1 and a_2, b_2 are initially in coherent states. For simplicity, we suppose that the initial state is prepared in a four-mode coherent state by using a Rabi rotation: $|\psi\rangle = |\frac{\alpha}{\sqrt{2}}\rangle_{a_1} |\frac{\alpha}{\sqrt{2}}\rangle_{a_2} |\frac{\alpha}{\sqrt{2}}\rangle_{b_1} |\frac{\alpha}{\sqrt{2}}\rangle_{b_2}$. After preparation, we assume that the inter-well potential is increased so that each well evolves independently, to give the solutions.

We have considered the conditions required to obtain the best squeezing of Schwinger spin operators by optimizing the phase choice θ (inset of Fig. 2). We set

$$\begin{aligned} \frac{\partial \Delta^2 \hat{J}^\theta}{\partial \theta} &= \frac{\partial}{\partial \theta} [\cos^2 \theta \Delta^2 \hat{J}^Z + \sin^2 \theta \Delta^2 \hat{J}^X \\ &\quad + 2 \cos \theta \sin \theta \langle \hat{J}^Z, \hat{J}^X \rangle] \\ &= 2 \cos(2\theta) \langle \hat{J}^Z, \hat{J}^X \rangle - \sin(2\theta) (\Delta^2 \hat{J}^Z - \Delta^2 \hat{J}^X) \\ &= 0 \end{aligned} \quad (\text{IV.6})$$

and therefore obtain as the optimal squeezing angle

$$\theta = \frac{1}{2} \arctan \left(\frac{2 \langle \hat{J}_A^Z, \hat{J}_A^X \rangle}{\Delta^2 \hat{J}_A^Z - \Delta^2 \hat{J}_A^X} \right), \quad (\text{IV.7})$$

where

$$\langle \hat{J}_A^Z, \hat{J}_A^X \rangle = \frac{1}{2} \left(\langle \hat{J}_A^Z \hat{J}_A^X \rangle + \langle \hat{J}_A^X \hat{J}_A^Z \rangle - 2 \langle \hat{J}_A^Z \rangle \langle \hat{J}_A^X \rangle \right). \quad (\text{IV.8})$$

The squeezing value in this case is:

$$S^{\theta, \theta+\pi/2} = \frac{\Delta^2 \hat{J}_A^{\theta, \theta+\pi/2}}{|\langle \hat{J}_A^Y \rangle|/2}, \quad (\text{IV.9})$$

where

$$\Delta^2 \hat{J}_A^\theta = \cos^2 \theta \Delta^2 \hat{J}_A^Z + \sin^2 \theta \Delta^2 \hat{J}_A^X + 2 \sin \theta \cos \theta \langle \hat{J}_A^Z, \hat{J}_A^X \rangle. \quad (\text{IV.10})$$

B. Producing the spatial entanglement

The next step, after generating the local squeezing at each well, is to decrease the inter-well potential for a short time, so that it acts as a controllable, non-adiabatic beam splitter [32], to allow interference between the wells; other methods of obtaining an effective beam-splitter could also be feasible.

Entanglement is generated by the interference of two squeezed states on a 50 : 50 beamsplitter with a relative optical phase of φ (Fig. 1). The resulting entangled modes are labelled by $c_{1,2}$ and $d_{1,2}$. Schwinger spin operators $\hat{J}_{C/D}^\theta$ are defined for these modes, in accordance with Eq. (IV.2). We note that $\hat{J}_C^{\theta, \theta+\pi/2}$, $\hat{J}_D^{\theta, \theta+\pi/2}$ are measurable locally, in the style necessary for an EPR experiment, by using Rabi rotations and number measurements.

The input-output relations for the Schwinger spin operators are given by $\hat{c} = t\hat{a} + re^{i\varphi}\hat{b}$, and $\hat{d} = t\hat{b} - re^{-i\varphi}\hat{a}$ with the amplitude reflection and transmission coefficients being denoted t and r . Here we use $\varphi = \pi/2$ and $r = t = 1/\sqrt{2}$. Thus:

$$\hat{c} = \frac{\hat{a} + i\hat{b}}{\sqrt{2}}, \quad \hat{d} = \frac{\hat{b} + i\hat{a}}{\sqrt{2}}. \quad (\text{IV.11})$$

The variances $\Delta^2(\hat{J}_C^\theta - \hat{J}_D^\theta)$ and $\Delta^2(\hat{J}_C^{\theta+\pi/2} + \hat{J}_D^{\theta+\pi/2})$ can *both* be small, so that

$$S_- = \Delta^2(\hat{J}_C^\theta - \hat{J}_D^\theta) < \frac{1}{2} (|\langle \hat{J}_C^Y \rangle| + |\langle \hat{J}_D^Y \rangle|) \quad (\text{IV.12})$$

and

$$S_+ = \Delta^2(\hat{J}_C^{\theta+\pi/2} + \hat{J}_D^{\theta+\pi/2}) < \frac{1}{2} (|\langle \hat{J}_C^Y \rangle| + |\langle \hat{J}_D^Y \rangle|),$$

the degree of variance reduction being limited only by the amount of squeezing in the input modes. This is the signature of EPR entanglement, in accordance with the entanglement criteria (II.2) and (II.3). In fact,

$$\begin{aligned} \Delta^2(\hat{J}_C^\theta \mp \hat{J}_D^\theta) &= \cos^2 \theta \Delta^2(\hat{J}_C^Z \mp \hat{J}_D^Z) + \sin^2 \theta \Delta^2(\hat{J}_C^X \mp \hat{J}_D^X) \\ &\quad + \cos \theta \sin \theta [\langle \hat{J}_C^Z \mp \hat{J}_D^Z, \hat{J}_C^X \mp \hat{J}_D^X \rangle \\ &\quad + \langle \hat{J}_C^X \mp \hat{J}_D^X, \hat{J}_C^Z \mp \hat{J}_D^Z \rangle]. \end{aligned} \quad (\text{IV.13})$$

A similar expression can be given for $\Delta^2(\hat{J}_C^{\theta'} \pm \hat{J}_D^{\theta'})$. The solutions show a reduction in these variances, for suitable

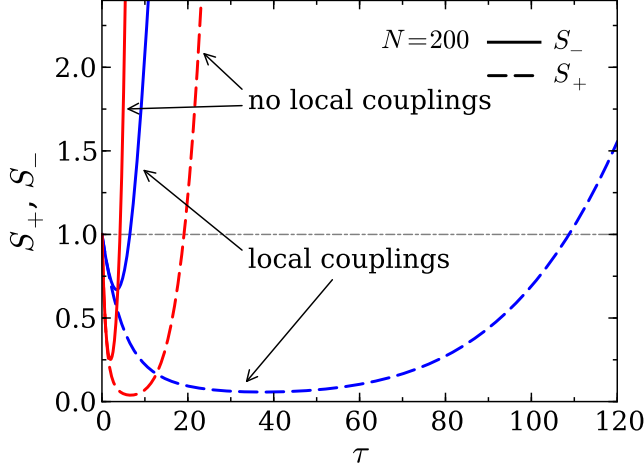


Figure 3. (Color online) Inference squeezing: $S_- = [\Delta^2(\hat{J}_C^\theta - \hat{J}_D^\theta)/n_0]$ (solid lines) and $S_+ = [\Delta^2(\hat{J}_C^{\theta+\pi/2} + \hat{J}_D^{\theta+\pi/2})/n_0]$ (dashed lines) after the beamsplitter interaction, where the shot noise level is $n_0 = (|\langle \hat{J}_C^Y \rangle| + |\langle \hat{J}_D^Y \rangle|)/2$. Here $N = N_A = N_B = 200$. The parameters are the same as Fig. 2. The red lines show the result without local cross couplings, i.e., $g_{12} = 0$, $g_{22} = g_{11}$.

parameters, to indicate that Alice can infer Bob's observable \hat{J}_C^θ (by measuring \hat{J}_D^θ) with increasing accuracy, as $\Delta^2(\hat{J}_C^\theta - \hat{J}_D^\theta) \rightarrow 0$. Similarly, she can infer the conjugate observable $\hat{J}_C^{\theta+\pi/2}$ (by measuring $\hat{J}_D^{\theta+\pi/2}$) to an increasing accuracy, as $\Delta^2(\hat{J}_C^{\theta+\pi/2} + \hat{J}_D^{\theta+\pi/2}) \rightarrow 0$. We call these variances “inference variances” to remind us of their role in the EPR paradox. Ideally, we want to find a regime for which both inference variances become very small.

It is convenient to express the output spin operators in terms of the inputs: we find

$$\begin{aligned} \hat{J}_C^Z - \hat{J}_D^Z &= \frac{i}{2} [\hat{a}_2^\dagger \hat{b}_2 - \hat{b}_2^\dagger \hat{a}_2 - \hat{a}_1^\dagger \hat{b}_1 + \hat{b}_1^\dagger \hat{a}_1], \\ \hat{J}_C^Z + \hat{J}_D^Z &= \frac{1}{2} [\hat{a}_2^\dagger \hat{a}_2 - \hat{a}_1^\dagger \hat{a}_1 + \hat{b}_2^\dagger \hat{b}_2 - \hat{b}_1^\dagger \hat{b}_1], \\ \hat{J}_C^X - \hat{J}_D^X &= \frac{i}{2} [e^{i(\theta_2 - \phi_1)} \hat{a}_2^\dagger \hat{b}_1 - e^{-i(\theta_1 - \phi_2)} \hat{b}_2^\dagger \hat{a}_1 \\ &\quad - e^{i(\theta_1 - \phi_2)} \hat{a}_1^\dagger \hat{b}_2 + e^{-i(\theta_2 - \phi_1)} \hat{b}_1^\dagger \hat{a}_2], \\ \hat{J}_A^Z + \hat{J}_B^Z &= \hat{J}_C^Z + \hat{J}_D^Z, \end{aligned} \quad (\text{IV.14})$$

where we have used $\theta_2 - \phi_2 = \theta_1 - \phi_1 = 0$ due to the symmetry of a and b , and $\theta_2 - \phi_1 = \theta_2 - \theta_1 = \pi/2 - \alpha$ as introduced for Eq. (IV.3). The solutions for the inference squeezing $\Delta^2(\hat{J}_C^\theta - \hat{J}_D^\theta)$ and $\Delta^2(\hat{J}_C^{\theta+\pi/2} + \hat{J}_D^{\theta+\pi/2})$ are shown in Fig. 3. We note that unlike for most EPR states, the inference variances are asymmetrical.

The spin orientation measured at each site can be selected independently to optimize the criterion for the state used. One can then show EPR entanglement via spin measurements by using the product entanglement

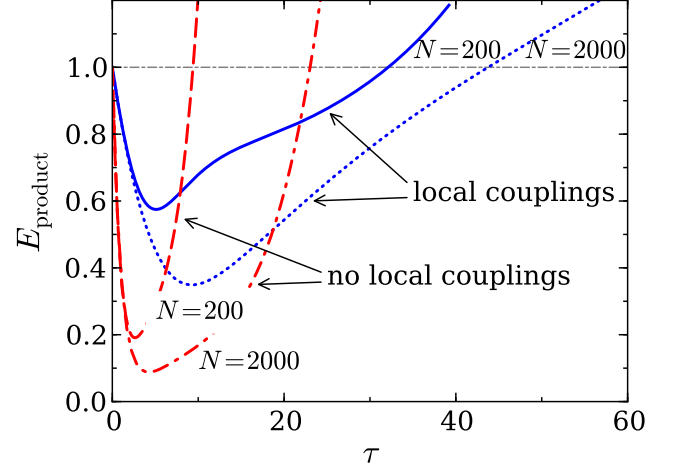


Figure 4. Entanglement ($E_{\text{product}} < 1$) based on the criterion in product form (IV.15). EPR paradox entanglement is obtained when $E_{\text{product}} < 0.5$. The solid and dotted lines stand for $N = N_A = N_B = 200$ and for $N = 2000$ with couplings corresponding to $B = 9.116$ G; while the dash-dotted and dashed lines assume no local cross couplings, i.e., $g_{12} = 0$, $g_{11} = g_{22}$, for $N = 200$ and for $N = 2000$.

criterion Eq. (II.3):

$$E_{\text{product}} = \frac{\sqrt{\Delta^2(\hat{J}_C^\theta - \hat{J}_D^\theta) \cdot \Delta^2(\hat{J}_C^{\theta+\pi/2} + \hat{J}_D^{\theta+\pi/2})}}{(|\langle \hat{J}_C^Y \rangle| + |\langle \hat{J}_D^Y \rangle|)/2} < 1. \quad (\text{IV.15})$$

After using the beam splitter, entanglement can be detected as $E_{\text{product}} < 1$, as shown in Fig. 4 by the solid curve, which assumes the couplings between spins found at the rubidium Feshbach resonance. Note that, consistent with the results found in previous studies of entanglement in the ground state, the dashed curve of Fig. 4 shows that no cross couplings, i.e., $g_{12} = 0$, gives much better results still. This would require spatially separated condensates for each spin orientation, in order to eliminate cross couplings, as recently demonstrated by using magnetic gradient techniques [48]. Fig. 4 reveals improvement in the entanglement, as one increases the number of atoms in the condensate.

C. EPR paradox entanglement

The entanglement predicted for the dynamical scheme is strong enough that it reveals an EPR paradox (steering) non-locality. This level of entanglement is reached when $E_{\text{product}} < 0.5$ (as shown in Section II), which occurs in the presence of local couplings for the larger atom numbers $N = 2000$, as shown in Fig. 4. The EPR paradox entanglement can be obtained for lower atom numbers $N \sim 200$ when local couplings are non-existent.

Next, we will examine the predictions for the more sensitive EPR criterion Eq. (II.4), which involves measure-

ments of the conditional variances. The EPR argument is based on an accuracy of inference, that an observer at D can predict the result \hat{J}_C^θ for an observer at C , to a certain measurable level of uncertainty. A simple way to determine an upper limit to this uncertainty is to use a linear estimate $g\hat{J}_D^\theta$, based on the result \hat{J}_D^θ for measurement at D . Then we arrive at the EPR paradox criterion of Eq. (II.7):

$$E_{\text{EPR-product}} = \frac{\sqrt{\Delta^2(\hat{J}_C^\theta - g\hat{J}_D^\theta) \cdot \Delta^2(\hat{J}_C^{\theta+\pi/2} + g'\hat{J}_D^{\theta+\pi/2})}}{|\langle \hat{J}_C^Y \rangle|/2} < 1, \quad (\text{IV.16})$$

which reduces to $E_{\text{product}} < 0.5$, for the choice $g = 1$. In fact, this choice of g is optimal where the inference squeezing is very strong.

We now determine how to optimize the choice of g , where the entanglement is weaker. The best choices for g and g' are adjusted to minimize $\Delta^2(\hat{J}_C^\theta - g\hat{J}_D^\theta)$ and $\Delta^2(\hat{J}_C^{\theta+\pi/2} + g'\hat{J}_D^{\theta+\pi/2})$. Following [35],

$$\begin{aligned} \frac{\partial}{\partial g} \Delta^2(\hat{J}_C^\theta - g\hat{J}_D^\theta) &= 2g\Delta^2\hat{J}_D^\theta - \langle \hat{J}_C^\theta, \hat{J}_D^\theta \rangle - \langle \hat{J}_D^\theta, \hat{J}_C^\theta \rangle \\ &= 0 \end{aligned} \quad (\text{IV.17})$$

implies the optimal g is given by

$$2g = (\langle \hat{J}_C^\theta, \hat{J}_D^\theta \rangle + \langle \hat{J}_D^\theta, \hat{J}_C^\theta \rangle) / \Delta^2\hat{J}_D^\theta. \quad (\text{IV.18})$$

We note $\langle \hat{J}_C^\theta, \hat{J}_D^\theta \rangle = \langle \hat{J}_D^\theta, \hat{J}_C^\theta \rangle$. There is similarly an optimum for the value of g' , with phase $\theta' = \theta + \pi/2$. Figure 5 shows the optimal value of factor g and g' with different cross couplings, versus time, for atoms $N_A = 200$.

Using the optimal values of the constants, one can evaluate the predictions for the variances, $\Delta^2(\hat{J}_C^\theta - g\hat{J}_D^\theta)$. We can express the required moments in terms of the moments of modes a , b , e.g.,

$$\begin{aligned} \hat{J}_C^Z - g\hat{J}_D^Z &= g_-(\hat{J}_A^Z + \hat{J}_B^Z) \\ &+ g_+ \left[\frac{\hat{a}_2^\dagger \hat{b}_2 - \hat{b}_2^\dagger \hat{a}_2 - \hat{a}_1^\dagger \hat{b}_1 + \hat{b}_1^\dagger \hat{a}_1}{2} \right], \end{aligned} \quad (\text{IV.19})$$

where we define $g_\pm = (1 \pm g)/2$, and use $\theta_2 - \phi_2 = \theta_1 - \phi_1 = 0$ due to the symmetry of a and b . The minimum variance is obtained by substitution of optimal g , Eq. (IV.18). One finds

$$\Delta^2(\hat{J}_C^Z - g\hat{J}_D^Z) = g_-^2 \Delta^2\hat{J}_+^Z + g_+^2 \Delta^2\hat{J}_-^Z, \quad (\text{IV.20})$$

where

$$\begin{aligned} \Delta^2\hat{J}_-^Z &= \Delta^2(\hat{J}_C^Z - \hat{J}_D^Z) \\ &= \Delta^2 \left(i \frac{\hat{a}_2^\dagger \hat{b}_2 - \hat{b}_2^\dagger \hat{a}_2 - \hat{a}_1^\dagger \hat{b}_1 + \hat{b}_1^\dagger \hat{a}_1}{2} \right), \\ \Delta^2\hat{J}_+^Z &= \Delta^2(\hat{J}_C^Z + \hat{J}_D^Z) = \Delta^2(\hat{J}_A^Z + \hat{J}_B^Z). \end{aligned} \quad (\text{IV.21})$$

Similarly

$$\begin{aligned} \hat{J}_C^X - g\hat{J}_D^X &= g_-(\hat{J}_A^X + \hat{J}_B^X) \\ &- g_+ \left[\frac{\hat{a}_2^\dagger \hat{b}_1 - \hat{b}_2^\dagger \hat{a}_1 + \hat{a}_1^\dagger \hat{b}_2 - \hat{b}_1^\dagger \hat{a}_2}{2} \right] \end{aligned} \quad (\text{IV.22})$$

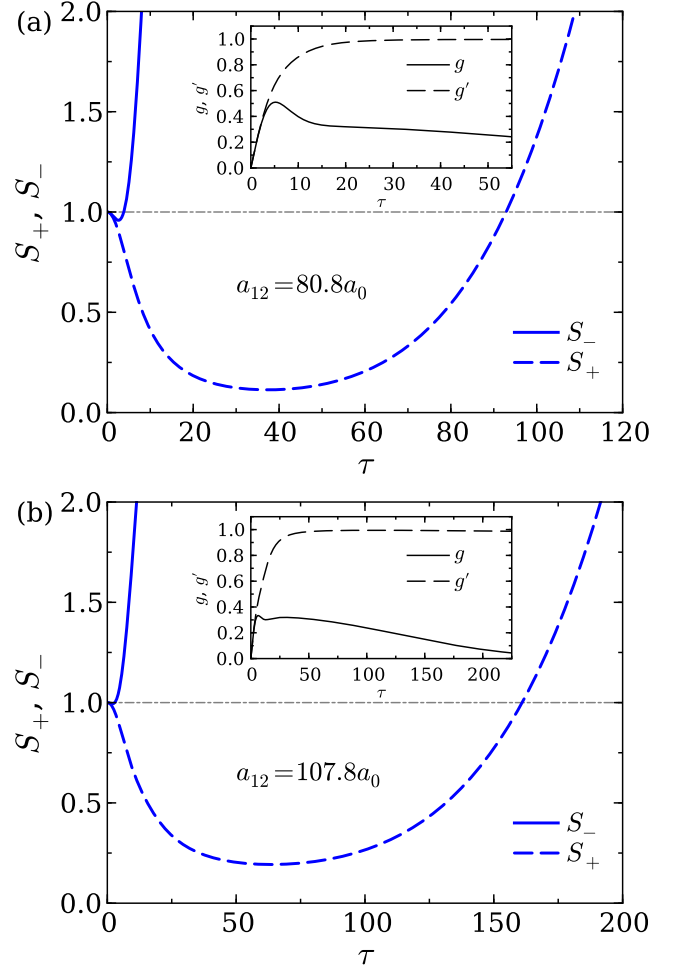


Figure 5. EPR paradox entanglement, shown by the simultaneous inference squeezing of $S_- = [\Delta^2(\hat{J}_C^\theta - g\hat{J}_D^\theta)/n_0]$ (solid lines) and $S_+ = [\Delta^2(\hat{J}_C^{\theta+\pi/2} + g'\hat{J}_D^{\theta+\pi/2})/n_0]$ (dashed lines) with optimal g and g' , where the shot noise level is $n_0 = (|\langle \hat{J}_C^Y \rangle|)/2$. Plots show different local cross couplings: (a) $B = 9.116$ G, and (b) $B = 9.086$ G. Insets show the optimal value of factors g (solid lines) and g' (dashed lines) with time. Here $N_A = N_B = 200$, and other parameters are as for Fig. 2.

with $\theta_2 - \phi_1 = -(\theta_1 - \phi_2) = \pi/2$, for which the minimum variance is

$$\Delta^2(\hat{J}_C^X - g\hat{J}_D^X) = g_-^2 \Delta^2\hat{J}_+^X + g_+^2 \Delta^2\hat{J}_-^X, \quad (\text{IV.23})$$

where

$$\begin{aligned} \Delta^2\hat{J}_-^X &= \Delta^2(\hat{J}_C^X - \hat{J}_D^X) \\ &= \Delta^2 \left(- \frac{\hat{a}_2^\dagger \hat{b}_1 - \hat{b}_2^\dagger \hat{a}_1 + \hat{a}_1^\dagger \hat{b}_2 - \hat{b}_1^\dagger \hat{a}_2}{2} \right), \\ \Delta^2\hat{J}_+^X &= \Delta^2(\hat{J}_C^X + \hat{J}_D^X) = \Delta^2(\hat{J}_A^X + \hat{J}_B^X). \end{aligned} \quad (\text{IV.24})$$

Also,

$$\begin{aligned} \langle \hat{J}_C^Z - g\hat{J}_D^Z, \hat{J}_C^X - g\hat{J}_D^X \rangle &= g_-^2 \langle \hat{J}_+^Z, \hat{J}_+^X \rangle \\ &+ g_+^2 \langle \hat{J}_-^Z, \hat{J}_-^X \rangle. \end{aligned} \quad (\text{IV.25})$$

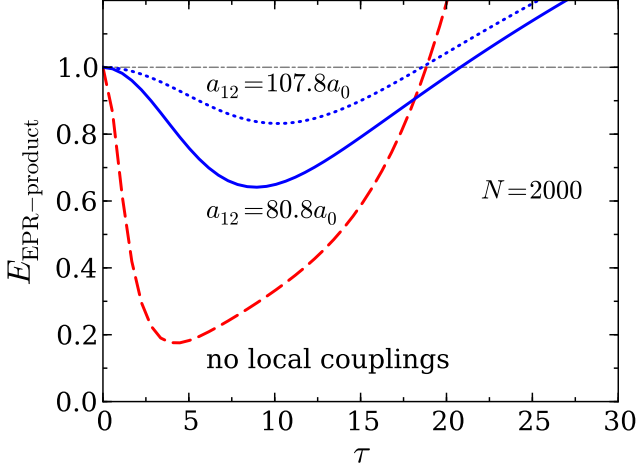


Figure 6. EPR paradox is predicted ($E_{\text{EPR-product}} < 1$), for a variety of local cross couplings. Here $N = N_A = N_B = 2000$; $B = 9.116$ G (solid line), $B = 9.086$ G (dotted line), and with no cross-couplings, i.e., $g_{12} = 0$, $g_{22} = g_{11}$ (dashed line). We use optimal value of factors g and g' for each case. Other parameters are as for the last figures.

The minimum interference squeezing $\Delta^2(\hat{J}_C^\theta - g\hat{J}_D^\theta)$ and $\Delta^2(\hat{J}_C^{\theta+\pi/2} + g'\hat{J}_D^{\theta+\pi/2})$ with optimal choices of g and g' are shown in Fig. 5. Unlike the original formulations of the EPR paradox, in this case, the two inference variances are asymmetric. The second inference variance exceeds the quantum limit for large enough τ . We note that for strong correlation as shown by S_+ over a large range of τ the optimal choice for g becomes 1. On the other hand, for the poor correlation shown by S_- as τ becomes larger, the optimal choice becomes $g' = 0$, so that the variance S_+ is limited to the variance of Bob's spin (Fig. 5).

Figure 6 shows regimes for which the EPR criteria are satisfied, i.e., $E_{\text{EPR-product}} < 1$, for different cross couplings. As the number of atoms increases, the spin squeezing increases and so too does the degree of EPR paradox, as shown in Fig. 7. The result is consistent with previous studies of the CV EPR paradox non-locality [8, 34]. An EPR paradox for the quadrature phase amplitudes of optical modes has been confirmed in a number of experiments [9]. Whether this effect is realizable for atoms however is a different question. Considerations include the size of τ compared to the decoherence time of the BEC condensate and whether interactions like nonlinear losses ignored in the model (IV.1) will come into play to reduce the EPR entanglement. To address these questions, we employ the stochastic truncated Wigner function technique valid for large N [33], in the next section.

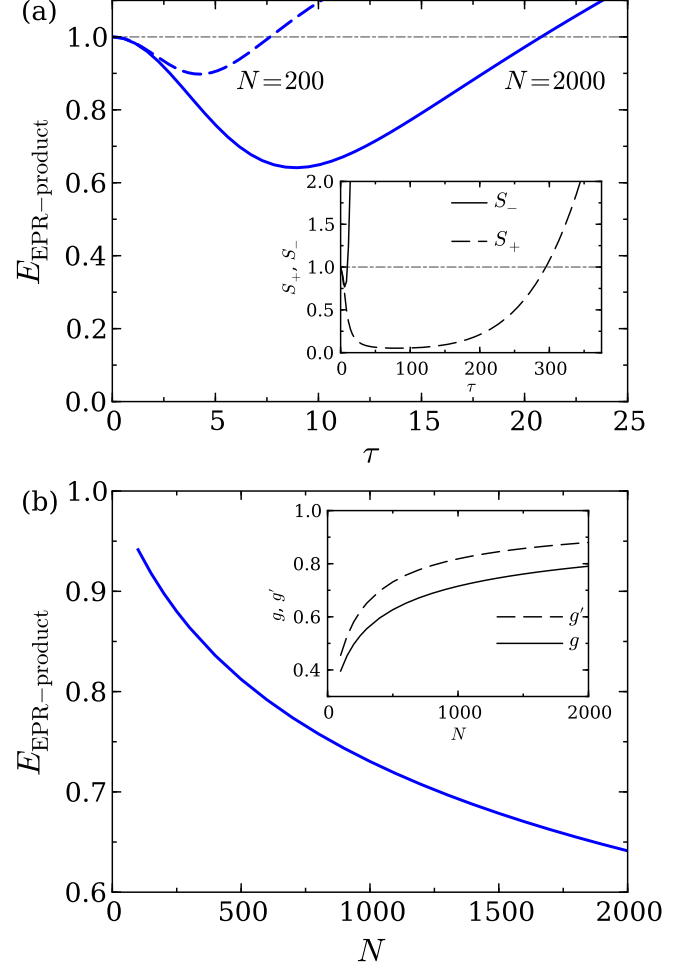


Figure 7. Effect of atom number: (a) $N = N_A = N_B = 200$ (dashed lines) and $N = 2000$ (solid lines) on the EPR paradox entanglement with optimal gain factors g and g' , for fixed couplings $B = 9.116$ G. Inset shows the individual squeezing inferences $S_- = [\Delta^2(\hat{J}_C^\theta - g\hat{J}_D^\theta)/n_0]$ (solid lines), $S_+ = [\Delta^2(\hat{J}_C^{\theta+\pi/2} + g'\hat{J}_D^{\theta+\pi/2})/n_0]$ (dashed lines) with optimal g and g' , for $N = 2000$. (b) The optimal $E_{\text{EPR-product}}$ versus different number of atoms. Inset shows the corresponding g , g' versus N .

V. STRATEGY II: SIMULTANEOUS EVOLUTION WITH TUNNELING PRESENT AND INCLUDING LOSSES

The degree of EPR entanglement is limited by the number of atoms (N) in the ensemble. Figure 7 shows a base value of ~ 0.83 for $N = 200$, but the entanglement improves to ~ 0.65 for $N = 2000$. However, the unitary evolution approach of the previous section becomes limited once dissipation effects are important. These effects are known to occur in ultra-cold atomic systems especially at high densities, due to spin-changing atomic collisions which cause density-dependent two-body and three-body losses. With this in mind we investigate the effect

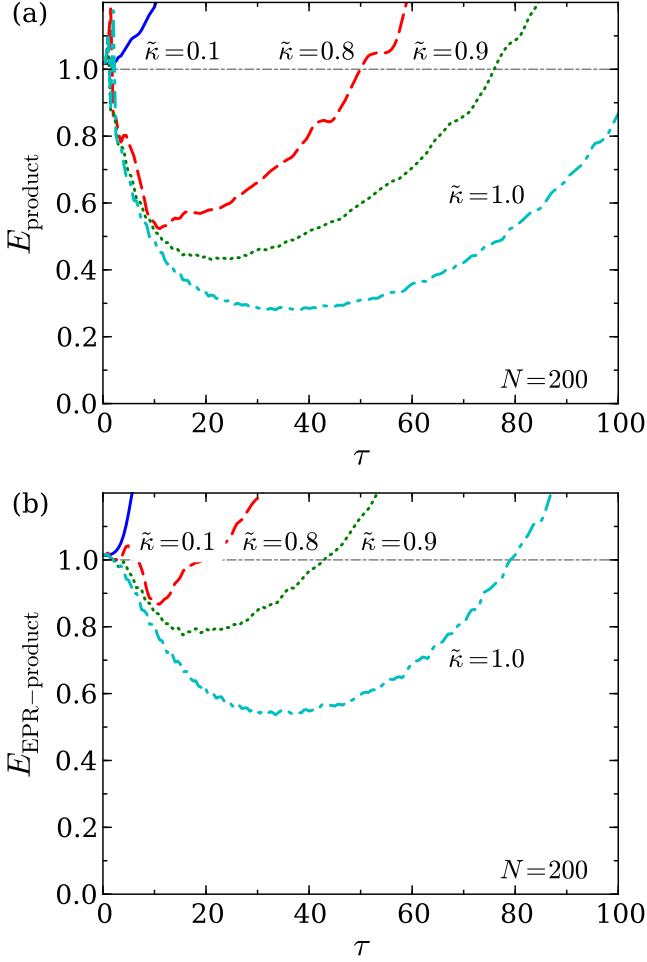


Figure 8. (Color online) Entanglement E_{product} (a) and $E_{\text{EPR-product}}$ (b) after evolution of the full Hamiltonian (III.2) including tunneling for $N = 200$ and $B = 9.116$ G, without the application of the beam splitter. The results are shown for values $\tilde{\kappa} = 0.1$ (blue solid lines), $\tilde{\kappa} = 0.8$ (red dashed lines), $\tilde{\kappa} = 0.9$ (green dotted lines) and $\tilde{\kappa} = 1$ (cyan dash-dotted lines).

tiveness of using a large number approximation, namely the truncated Wigner function technique [33]. In this approach, higher order terms in $1/N^{3/2}$ are ignored, to allow a stochastic calculation based on a positive Wigner function. This method readily scales to large numbers of atoms and modes [49], and can include nonlinear losses. The detailed description of the method can be found in Appendix B.

The predictions of the truncated Wigner method are indistinguishable from the exact method given in Appendix A in the case of zero losses and no tunneling, which confirms its validity for $N \sim 200$ –2000. The advantage of the Wigner method is that it allows a ready solution of the dynamics of the full Hamiltonian (III.1, III.2) where both tunneling and nonlinear terms are present, even for large atom numbers. The method also allows the inclusion of losses, which are

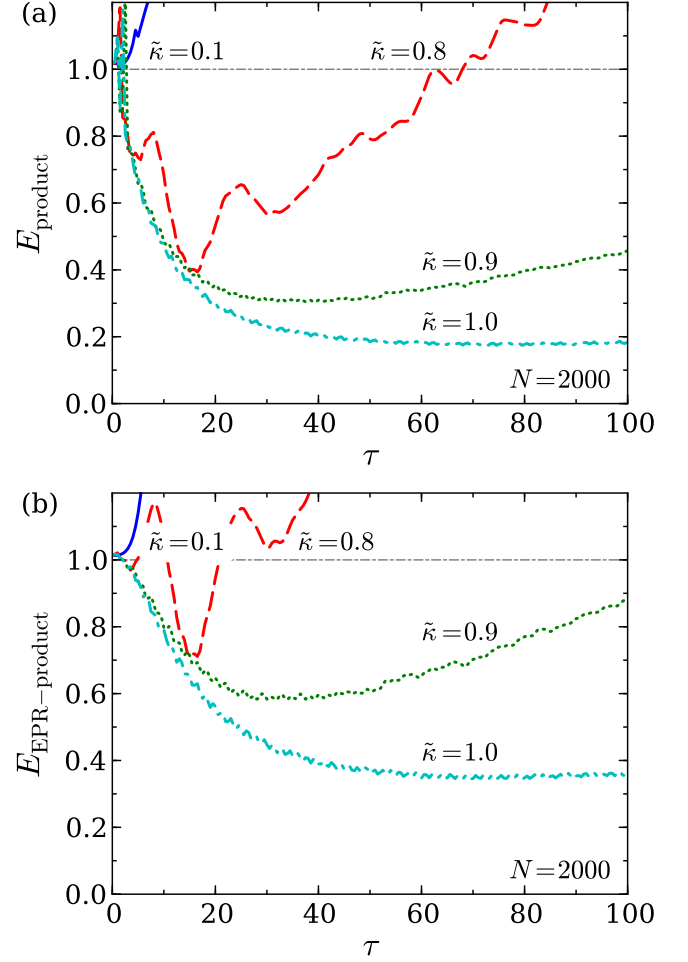


Figure 9. (Color online) Entanglement E_{product} (a) and $E_{\text{EPR-product}}$ (b) after evolution of the full Hamiltonian (III.2) including tunneling for $N = 2000$ and $B = 9.116$ G. Meaning of the lines is the same as in Fig. 8.

known to destroy squeezing and entanglement, and will come into play in realistic experimental arrangements. For example, tunneling cannot be completely suppressed, and also potentially significant is the role of nonlinear loss, that will come into play with large atom numbers.

Once tunneling is present in the nonlinear Hamiltonian, entanglement can be created between the two modes, *without* the second beam splitter step described in Section IV. Figure 8 shows the effect of tunneling on the entanglement. Strong tunneling ($\tilde{\kappa} \sim 1$, i.e., with the strength of the same order as the nonlinear interaction) produces significant entanglement even without the final application of the beam splitter. However, tunneling this strong is hard to achieve in a simple two-well BEC experiment, where values of $\tilde{\kappa} \sim 10^{-3} \dots 10^{-2}$ are more common. The achievement of such large couplings is likely to require a more sophisticated experimental design.

If one increases the number of atoms N , with the absence of losses the dimensionless drift part of equa-

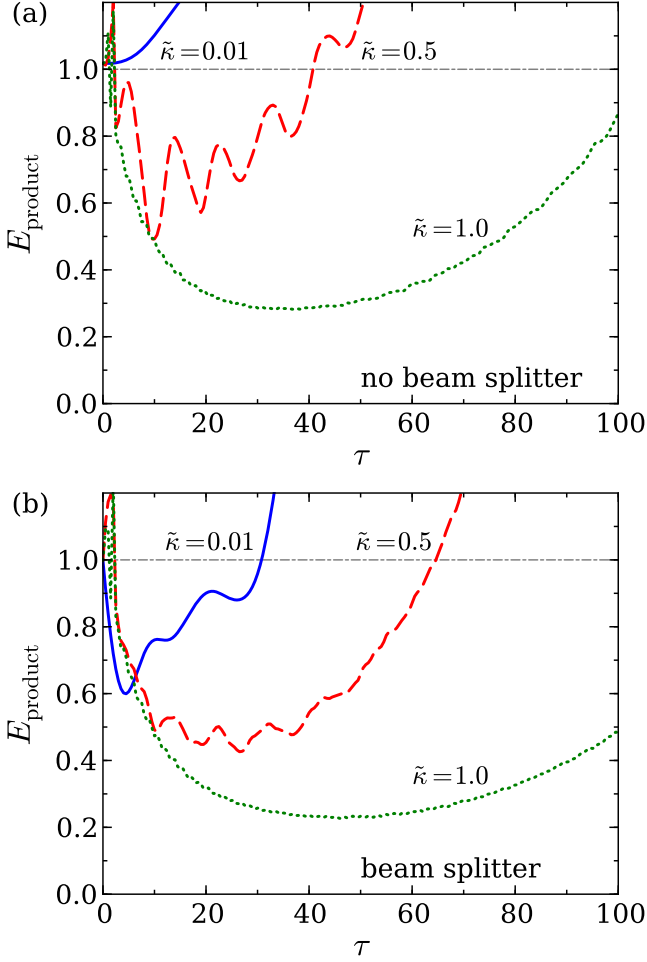


Figure 10. (Color online) Entanglement E_{product} after evolution of the full Hamiltonian (III.2) including tunneling for $N = 200$ and $B = 9.116$ G, (a) without and (b) with the application of the beam splitter. The results are shown for values $\tilde{\kappa} = 0.01$ (blue solid lines), $\tilde{\kappa} = 0.5$ (red dashed lines), and $\tilde{\kappa} = 1$ (green dotted lines).

tions (B.4) will stay the same, but the results will differ, as shown in Fig. 9. The entanglement improves with higher N , as in the case of the two-step strategy and as found previously for ground state calculations. This result is consistent for continuous variable EPR entanglement, which has been predicted in optics for high intensity Gaussian states.

We also analyze the predictions for entanglement with the insertion of step 2, the “beam splitter” interaction described in Section IV.B, the objective being to understand whether a small amount of tunneling and nonlinear loss present in the first interaction stage will detract from the amount of entanglement that is predicted by the two-step strategy. We focus on the case where local couplings are present, although this gives a worse case prediction for entanglement. The losses and tunneling tend to detract from the amount of entanglement, so that in the case of 2000 atoms, with local couplings, an entangle-

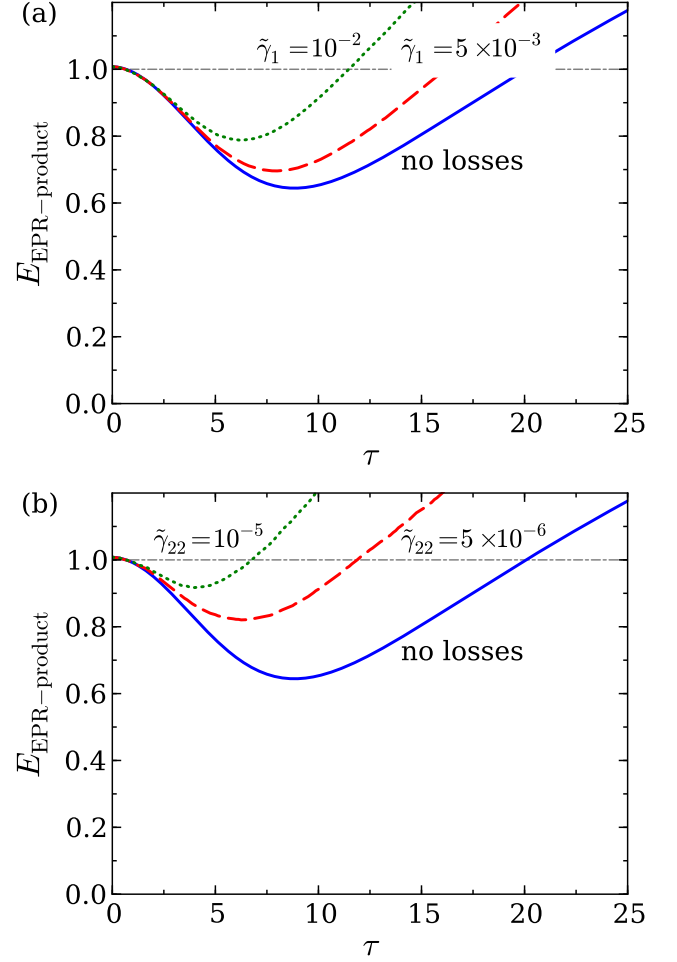


Figure 11. (Color online) EPR paradox entanglement as measured by $E_{\text{EPR-product}}$ without tunneling and with the application of the beam splitter, for $B = 9.116$ G and $N_A = N_B = 2000$. (a) Only linear losses are enabled; no losses (solid blue lines), $\tilde{\gamma}_1 = 5 \times 10^{-3}$ (dashed red lines), $\tilde{\gamma}_1 = 10^{-2}$ (dotted green lines). (b) Only two-body intra-species losses are enabled; no losses (solid blue lines), $\tilde{\gamma}_{22} = 5 \times 10^{-6}$ (dashed red lines), $\tilde{\gamma}_{22} = 10^{-5}$ (dotted green lines).

ment of ~ 0.4 (enough to give an EPR paradox) as shown in Fig. 4 is reduced to ~ 0.6 (Fig. 10). We emphasize here that losses are highly adjustable through changes in density, so these issues are more related to appropriate experimental design than to fundamental limits. The application of the beam splitter improves entanglement significantly when tunneling is weak, but with $\tilde{\kappa}$ values close to 1 tunneling becomes the prevalent source of entanglement, as illustrated in Fig. 10.

The presence of linear losses, or intra-species losses decreases the maximum entanglement, as shown in Fig. 11. But when the nonlinear inter-species losses are enabled, our simulations show that they unexpectedly *increase* the entanglement (Fig. 12).

We have found that this only occurs with a nonlinear loss $\tilde{\gamma}_{12}$ that specifically couples the two species together.

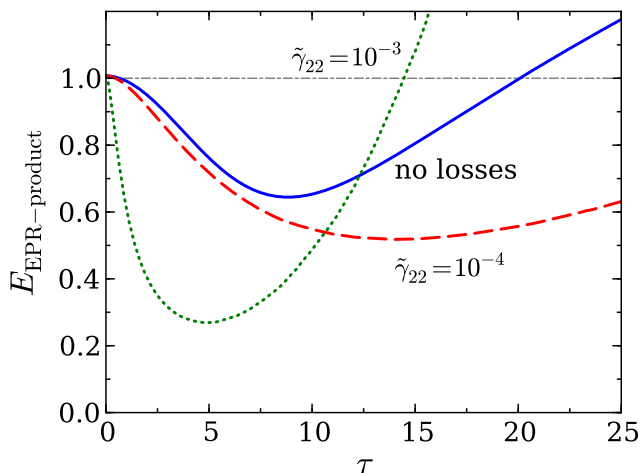


Figure 12. (Color online) EPR paradox entanglement as measured by $E_{\text{EPR-product}}$ without tunneling and with the application of the beam splitter, for $B = 9.116 \text{ G}$ and $N_A = N_B = 2000$. Only two-body inter-species losses are enabled; no losses (solid blue lines), $\tilde{\gamma}_{12} = 10^{-4}$ (dashed red lines), $\tilde{\gamma}_{12} = 10^{-3}$ (dotted green lines).

Other forms of loss, including linear loss, will simply reduce the entanglement — as one expects from decoherence effects. Generating entanglement by a manipulation of reservoirs has been observed for atomic ensembles [50]. The process in our case appears to be related to the fact that nonlinear absorption just by itself is known to create a nonclassical state [51], which can then become entangled through linear couplings alone.

VI. SUMMARY

In summary, we have analyzed two strategies for dynamical preparation of squeezed and entangled atomic states, through the use of nonlinear interactions that rely on the naturally occurring S-wave interactions between trapped atoms. The possible advantage of the methods proposed here is that they do not require the use of separate local oscillators, as often employed in optics for measuring entanglement. These could be potentially technically difficult to use in some cold-atom systems, due to dephasing that is caused by interatomic interactions in the local-oscillator itself, when combined with number fluctuations. However, atomic homodyning has recently been realised [3], and may present a better strategy in some cases, particularly where it is important to avoid local cross-couplings. Work done in parallel with ours studies the dynamical preparation of entanglement for this case, using a single mode at each well [52].

We find that robust spatial entanglement and EPR inference is possible under the correct conditions, even including Poissonian number fluctuations. These effects are also not greatly perturbed by realistic loss values. In fact, with the presence of certain types of inter-species

loss, we calculate that enhanced entanglement is possible. Finally, we note that the optimum regime is for rather large coupling or tunneling values between the spatial modes, which appears to require a different experimental design to a simple two-well system.

The EPR paradox entanglement studied in this paper confirms an inconsistency of local realism with the completeness of quantum mechanics [7], and is evidence for the form of nonlocality called “steering” [10]. We make the point however that EPR entanglement is not itself sufficient to imply a direct failure of local realism, as would be demonstrated by a violation of a Bell inequality [6, 8]. The method employed to arrive at the predictions of EPR entanglement illustrates this point, since the truncated Wigner function is positive, and therefore provides a local hidden variable theory to describe the statistics of experiments where the measurement is effectively that of a quadrature phase amplitude, even though significant EPR entanglement can be obtained [8]. The distinction between the EPR steering and Bell forms of nonlocality has been emphasised further in recent papers [11].

ACKNOWLEDGMENTS

We wish to thank the Australian Research Council for funding via ACQAO COE, Discovery and DECRA grants, as well as useful discussions with M. Oberthaler, P. Treutlein and A. Sidorov.

Appendix A: Exact dynamical solutions

a. One-mode model:

We start by considering a simple nonlinear, single-mode interaction that occurs locally at each well, and is modeled by Hamiltonian

$$\hat{H}/\hbar = \frac{g}{2} : \hat{N}^2 : . \quad (\text{A.1})$$

In order to understand the dynamics induced by the above Hamiltonian, we calculate results in the Heisenberg picture, where one obtains:

$$\frac{d\hat{a}_i}{dt} = \frac{i}{\hbar} [\hat{H}, \hat{a}_i] = -ig\hat{a}^\dagger \hat{a} \hat{a} = -ig\hat{N}\hat{a}. \quad (\text{A.2})$$

Since the number of particles is conserved, this has the solution:

$$\hat{a}(t) = \exp[-ig\hat{N}t] \hat{a}(0), \quad (\text{A.3})$$

which gives

$$\begin{aligned}
\langle \hat{a}(t) \rangle &= \langle \Psi(0) | \hat{a}(t) | \Psi(0) \rangle \\
&= \sum_{n,m=0}^{\infty} C_n^* C_m \langle n | \exp[-ig\hat{N}t] \hat{a}(0) | m \rangle \\
&= \sum_{n=0}^{\infty} C_n^* C_{n+1} \sqrt{n+1} \exp[-ignt] \\
&= \alpha e^{-|\alpha|^2} \sum_{n=0}^{\infty} e^{-ignt} \frac{|\alpha|^{2n}}{n!} \\
&= \alpha \exp[|\alpha|^2 (e^{-igt} - 1)]. \tag{A.4}
\end{aligned}$$

This predicts a well-known behavior with three characteristic time scales:

- On very short time scales, there is simply an oscillation with a renormalized frequency of $\omega' = g\bar{n}$, where $\bar{n} = |\alpha|^2$. A similar result is obtained classically.
- On intermediate time-scales, there is a quadratic damping, with a characteristic damping rate of $g\sqrt{\bar{n}}$, which is proportional to the standard deviation in the initial particle number.
- Finally, on very long time-scales there is a succession of periodic revivals where the initial state and all its properties are regained exactly, apart from a possible phase-shift. This occurs whenever $t = 2\pi/g$.

b. Two-mode model:

Next, consider a simple two-mode model, with two internal (spin) modes, where the Hamiltonian for the coupled system is:

$$\hat{H} = \frac{\hbar}{2} \sum_{ij} g_{ij} \hat{a}_i^\dagger \hat{a}_j^\dagger \hat{a}_j \hat{a}_i = \frac{\hbar}{2} : \sum_{ij} g_{ij} \hat{N}_i \hat{N}_j :. \tag{A.5}$$

We can solve this using either Schroedinger or Heisenberg equations of motion. In the Heisenberg case, one obtains:

$$\frac{d\hat{a}_i}{dt} = \frac{i}{\hbar} [\hat{H}, \hat{a}_i] = -i \sum_j g_{ij} \hat{a}_j^\dagger \hat{a}_j \hat{a}_i = -i \sum_j g_{ij} \hat{N}_j \hat{a}_i. \tag{A.6}$$

Since the number of particles is conserved in each mode, this has the solution:

$$\hat{a}_i(t) = \exp \left[-i \sum_j g_{ij} \hat{N}_j t \right] \hat{a}_i(0). \tag{A.7}$$

We suppose the initial quantum state factorizes into a vacuum state in one mode and coherent state in the

second, and that the condensate mode is give by:

$$|\Psi(0)\rangle = |0\rangle_{a_1} |\alpha\rangle_{a_2} = |0\rangle_{a_1} \sum_{n=0}^{\infty} C_n |n\rangle_{a_2}, \tag{A.8}$$

which gives

$$\begin{aligned}
\hat{a}_1^\dagger \hat{a}_1 |\Psi(0)\rangle &= 0, \\
\hat{a}_2^\dagger \hat{a}_2 |\Psi(0)\rangle &= |\alpha|^2 |\Psi(0)\rangle. \tag{A.9}
\end{aligned}$$

In this coherent state the number fluctuation variance is N . Suppose we apply a linear beamsplitter, then, after the beam-splitter:

$$\begin{aligned}
\bar{a}_1 &= \frac{1}{\sqrt{2}} (\hat{a}_1 + \hat{a}_2), \\
\bar{a}_2 &= \frac{1}{\sqrt{2}} (\hat{a}_2 - \hat{a}_1), \tag{A.10}
\end{aligned}$$

the state becomes

$$|\bar{\Psi}(0)\rangle = \left| \frac{\alpha}{\sqrt{2}} \right\rangle_{a_1} \left| \frac{\alpha}{\sqrt{2}} \right\rangle_{a_2}. \tag{A.11}$$

After the application of the nonlinear Hamiltonian (A.5), squeezing is generated locally, and

$$\begin{aligned}
\langle \bar{a}_i(t) \rangle &= \langle \bar{\Psi}(0) | \bar{a}_i(t) | \bar{\Psi}(0) \rangle \\
&= \left\langle \frac{\alpha}{\sqrt{2}} \right| \left\langle \frac{\alpha}{\sqrt{2}} \right| \exp \left[-i \sum_j g_{ij} \hat{N}_j t \right] \bar{a}_i \left| \frac{\alpha}{\sqrt{2}} \right\rangle \left| \frac{\alpha}{\sqrt{2}} \right\rangle \\
&= \sum_{n_1, n_2, m_1, m_2=0}^{\infty} C_{n_1}^* C_{n_2}^* C_{m_1} C_{m_2} \\
&\quad \times \langle n_1 | \langle n_2 | \exp \left[-i \sum_j g_{ij} \hat{N}_j t \right] \bar{a}_i | m_1 \rangle | m_2 \rangle \\
&= \frac{\alpha}{\sqrt{2}} \exp \left[\frac{|\alpha|^2}{2} (e^{-ig_{i1}t} - 1) \right] \exp \left[\frac{|\alpha|^2}{2} (e^{-ig_{i2}t} - 1) \right]. \tag{A.12}
\end{aligned}$$

We wish to calculate the phase variance in $\hat{\theta} \equiv \hat{\theta}_1 - \hat{\theta}_2$, as this gives rise to the decay in an interference pattern:

$$\langle (\Delta\hat{\theta})^2 \rangle \equiv \langle \hat{\theta}^2 \rangle - \langle \hat{\theta} \rangle^2. \tag{A.13}$$

Appendix B: Truncated Wigner Method

Including losses, the master equation in four-mode approximation is written as

$$\frac{d\hat{\rho}}{dt} = -\frac{i}{\hbar} [\hat{H}, \hat{\rho}] + \sum_l \gamma_l \mathcal{L}_l[\hat{\rho}], \tag{B.1}$$

where the Hamiltonian is defined as (III.2), and loss term has the form

$$\mathcal{L}_l[\hat{\rho}] = 2\hat{O}_l \hat{\rho} \hat{O}_l^\dagger - \hat{O}_l^\dagger \hat{O}_l \hat{\rho} - \hat{\rho} \hat{O}_l^\dagger \hat{O}_l. \tag{B.2}$$

We consider three different sources of losses: $\hat{O}_{22A} = \hat{a}_2^2$ and $\hat{O}_{22B} = \hat{b}_2^2$ (two-body intra-species loss), $\hat{O}_{12A} = \hat{a}_1\hat{a}_2$ and $\hat{O}_{12B} = \hat{b}_1\hat{b}_2$ (two-body inter-species loss), $\hat{O}_{1A} = \hat{a}_2$ and $\hat{O}_{1B} = \hat{b}_1$ (linear loss).

In order to further normalize the equation (B.1), we use the dimensionless time $\tau = g_{11}N_A t$ introduced in Section III. This gives us the dimensionless master equation

$$\frac{d\hat{\rho}}{d\tau} = -i[\tilde{H}, \hat{\rho}] + \sum_l \tilde{\gamma}_l \mathcal{L}_l[\hat{\rho}], \quad (\text{B.3})$$

with a dimensionless Hamiltonian \tilde{H} as in Eq. (III.3), and dimensionless loss coefficients $\tilde{\gamma}_l = \gamma_l/g_{11}N_A$. This equation can be transformed to the equivalent partial differential equation by applying the Wigner transformation [33]:

$$\begin{aligned} \mathcal{W}[\hat{A}] &= \frac{1}{\pi^8} \int d^2\lambda_1 d^2\lambda_2 d^2\lambda_3 d^2\lambda_4 \\ &\times \left(\prod_{i=1}^4 \exp(-\lambda_i z_i^* + \lambda_i^* z_i) \right) \\ &\times \text{Tr} \left\{ \hat{A} \prod_{i=1}^4 \exp(\lambda_i \hat{z}_i^\dagger - \lambda_i^* \hat{z}_i) \right\}, \end{aligned}$$

where 4-vectors $\mathbf{z}^T = (\alpha_1 \ \beta_1 \ \alpha_2 \ \beta_2)$ and $\hat{\mathbf{z}}^T = (\hat{a}_1 \ \hat{b}_1 \ \hat{a}_2 \ \hat{b}_2)$ were introduced for convenience. The resulting differential equation, after truncating higher-order derivatives, is a Fokker-Planck equation (FPE) for the truncated (positive) Wigner function $W \equiv \mathcal{W}[\hat{\rho}]$

$$\frac{dW}{d\tau} = -\partial_{\mathbf{z}}^T \mathbf{a} W - \partial_{\mathbf{z}^*}^T \mathbf{a}^* W + \text{Tr} \{ \partial_{\mathbf{z}} \partial_{\mathbf{z}^*}^T B B^H \} W,$$

where

$$\mathbf{z}^T = (\alpha_1 \ \beta_1 \ \alpha_2 \ \beta_2),$$

$$\partial_{\mathbf{z}}^T = \left(\frac{\partial}{\partial \alpha_1} \ \frac{\partial}{\partial \beta_1} \ \frac{\partial}{\partial \alpha_2} \ \frac{\partial}{\partial \beta_2} \right),$$

$$\mathbf{a} = -i\mathbf{a}_{\text{drift}} - \mathbf{a}_{\text{loss}},$$

$$\mathbf{a}_{\text{drift}} = \begin{pmatrix} \tilde{\kappa}_1 \beta_1 + \alpha_1 \{ \tilde{g}_{11} |\alpha_1|^2 + \tilde{g}_{12} |\alpha_2|^2 \} \\ \tilde{\kappa}_1 \alpha_1 + \beta_1 \{ \tilde{g}_{11} |\beta_1|^2 + \tilde{g}_{12} |\beta_2|^2 \} \\ \tilde{\kappa}_2 \beta_2 + \alpha_2 \{ \tilde{g}_{12} |\alpha_1|^2 + \tilde{g}_{22} |\alpha_2|^2 \} \\ \tilde{\kappa}_2 \alpha_2 + \beta_2 \{ \tilde{g}_{12} |\beta_1|^2 + \tilde{g}_{22} |\beta_2|^2 \} \end{pmatrix},$$

$$\mathbf{a}_{\text{loss}} = \begin{pmatrix} \alpha_1 \{ \tilde{\gamma}_{12} |\alpha_2|^2 + \tilde{\gamma}_1 \} \\ \beta_1 \{ \tilde{\gamma}_{12} |\beta_2|^2 + \tilde{\gamma}_1 \} \\ \alpha_2 \{ \tilde{\gamma}_{12} |\alpha_1|^2 + 2\tilde{\gamma}_{22} |\alpha_2|^2 \} \\ \beta_2 \{ \tilde{\gamma}_{12} |\beta_1|^2 + 2\tilde{\gamma}_{22} |\beta_2|^2 \} \end{pmatrix},$$

$$B = \begin{pmatrix} \sqrt{\tilde{\gamma}_{12}} \alpha_2 & 0 & 0 & 0 & \sqrt{\tilde{\gamma}_1} & 0 \\ 0 & \sqrt{\tilde{\gamma}_{12}} \beta_2 & 0 & 0 & 0 & \sqrt{\tilde{\gamma}_1} \\ \sqrt{\tilde{\gamma}_{12}} \alpha_1 & 0 & \sqrt{\tilde{\gamma}_{22}} \alpha_2 & 0 & 0 & 0 \\ 0 & \sqrt{\tilde{\gamma}_{12}} \beta_1 & 0 & \sqrt{\tilde{\gamma}_{22}} \beta_2 & 0 & 0 \end{pmatrix}.$$

This FPE is equivalent to the following set of stochastic differential equations (SDEs) [53]:

$$d\mathbf{z} = \mathbf{a} d\tau + B d\mathbf{Z}, \quad (\text{B.4})$$

where $d\mathbf{Z}^T = (dZ_{12A} \ dZ_{12B} \ \dots \ dZ_{1A} \ dZ_{1B})$ is a complex 6-dimensional Wiener process. These equations can be solved numerically using conventional methods, and their solution can, in turn, be used to get the expectations of symmetrically ordered operator products as

$$\begin{aligned} \langle \{ (\hat{a}_i^\dagger)^m \hat{a}_j^n \dots \}_{\text{sym}} \rangle &= \int (\alpha_i^*)^m \alpha_j^n \dots W d^2\mathbf{z} \\ &\approx \langle (\alpha_i^*)^m \alpha_j^n \dots \rangle_{\text{paths}}, \end{aligned}$$

where $\langle \rangle_{\text{paths}}$ stands for the average over the simulation paths.

As for Section III, we assume the initial state to be the coherent state:

$$|\psi\rangle = |\alpha_0\rangle_{a_1} |\alpha_0\rangle_{a_2} |\beta_0\rangle_{b_1} |\beta_0\rangle_{b_2}, \quad (\text{B.5})$$

where $\alpha_0 = \sqrt{N_A/2}$, $\beta_0 = \sqrt{N_B/2}$. Therefore

$$\alpha_i = \alpha_0 + \frac{1}{2}\eta_{1i}, \quad \beta_i = \beta_0 + \frac{1}{2}\eta_{2i},$$

where η_{1i} and η_{2i} are complex normally distributed random numbers with $\langle \eta_{ji}^* \eta_{kl} \rangle = \delta_{jk} \delta_{il}$.

-
- [1] B. Julsgaard, A. Kozhekin, and E. S. Polzik, *Nature* **413**, 400 (2001).
 - [2] R. Bücker, J. Grond, S. Manz, T. Berrada, T. Betz, C. Koller, U. Hohenester, T. Schumm, A. Perrin, and J. Schmiedmayer, *Nature Physics* **7**, 608 (2011).
 - [3] C. Gross, H. Strobel, E. Nicklas, T. Zibold, N. Bargill, G. Kurizki, and M. K. Oberthaler, *Nature* **480**, 219 (2011).
 - [4] B. Lücke, M. Scherer, J. Kruse, L. Pezzé, F. Deuretzbacher, P. Hyllus, O. Topic, J. Peise, W. Ertmer, J.

Arlt, L. Santos, A. Smerzi, and C. Klempt, *Science* **334**, 773 (2011).

- [5] W. Marshall, C. Simon, R. Penrose, and D. Bouwmeester, *Phys. Rev. Lett.* **91**, 130401 (2003); A. J. Leggett, *J. Phys.: Condens. Matter* **14** (15), R415 (2002); J. Z. Bernad, L. Diosi, and T. Geszti, *Phys. Rev. Lett.* **97**, 250404 (2006).
- [6] J. S. Bell, *Physics*, **1**, 195 (1965); J. F. Clauser, M. A.

- Horne, A. Shimony, and R. A. Holt, Phys. Rev. Lett. **23**, 880 (1969); J. F. Clauser and A. Shimony, Rep. Prog. Phys. **41**, 1881 (1978); A. Aspect, P. Grangier, and G. Roger, Phys. Rev. Lett. **49**, 91 (1982); A. Aspect, J. Dalibard, and G. Roger, Phys. Rev. Lett. **49**, 1804 (1982); P. G. Kwiat et al, *ibid.* **75**, 4337 (1995); G. Weihs et al, *ibid.* **81**, 5039 (1998); W. Tittel et al, *ibid.* **84**, 4737 (2000).
- [7] A. Einstein, B. Podolsky, and N. Rosen, Phys. Rev. **47**, 777 (1935).
- [8] Z. Y. Ou et al, Phys. Rev. Lett. **68**, 3663 (1992).
- [9] M. D. Reid et al, Rev. Mod. Phys. **81**, 1727 (2009).
- [10] H. M. Wiseman, S. J. Jones, and A. C. Doherty, Phys. Rev. Lett. **98**, 140402 (2007); S. J. Jones, H. M. Wiseman, and A. C. Doherty, Phys. Rev. A **76**, 052116 (2007); D. J. Saunders, S. J. Jones, H. M. Wiseman, and G. J. Pryde, Nature Physics **6**, 845 (2010).
- [11] E. G. Cavalcanti, S. J. Jones, H. M. Wiseman, and M. D. Reid, Phys. Rev. A **80**, 032112 (2009); E. G. Cavalcanti, Q. Y. He, M. D. Reid, and H. M. Wiseman, Phys. Rev. A **84**, 032115 (2011).
- [12] D. H. Smith et al, Nature Commu. **3**, 625 (2012); B. Wittmann et al, arXiv:1111.0760v3; A. J. Bennet et al, e-print arXiv:1111.0739.
- [13] T. Opatrny and G. Kurizki, Phys. Rev. Lett. **86**, 3180 (2001); K.V. Kheruntsyan and P. D. Drummond, Phys. Rev. A **66**, 031602(R) (2002); K. V. Kheruntsyan, M. K. Olsen, and P. D. Drummond, Phys Rev Lett. **95**, 150405 (2005).
- [14] J.-C. Jaskula et al, Phys. Rev. Lett. **105**, 190402 (2010); V. Krachmalnicoff et al, Phys. Rev. Lett. **104**, 150402 (2010).
- [15] J. M. Vogels, K. Xu, and W. Ketterle, Phys. Rev. Lett. **89**, 020401 (2002).
- [16] A. A. Norrie, R. J. Ballagh, and C. W. Gardiner, Phys. Rev. Lett. **94**, 040401 (2005); P. Deuar and P. D. Drummond, Phys. Rev. Lett. **98**, 120402 (2007).
- [17] N. Bar-Gill et al, Phys. Rev. Lett. **106**, 120404 (2011).
- [18] Q. Y. He, M. D. Reid, T. G. Vaughan, C. Gross, M. Oberthaler, and P. D. Drummond, Phys. Rev. Lett. **106**, 120405 (2011).
- [19] A. J. Ferris, M. K. Olsen, E. G. Cavalcanti, and M. J. Davis, Phys. Rev. A **78**, 060104 (2008); A. J. Ferris, M. K. Olsen, and M. J. Davis, Phys. Rev. A **79**, 043634 (2009).
- [20] P. Milman, A. Keller, E. Charon, and O. Atabek, Phys. Rev. Lett. **99**, 130405 (2007); Magnus Ögren and K. V. Kheruntsyan Phys. Rev. A **82**, 013641 (2010).
- [21] J. Esteve, C. Gross, A. Weller, S. Giovanazzi, and M. K. Oberthaler, Nature **455**, 1216 (2008).
- [22] T. Aoki et al, Phys. Rev. Lett. **91**, 080404 (2003).
- [23] A. Ekert, Phys. Rev. Lett. **67**, 661 (1991); J. Barrett, L. Hardy, and A. Kent, Phys Rev Lett **95**, 010503 (2005); A. Acin et al, Phys Rev Lett **98**, 230501 (2007).
- [24] H. Lee, P. Kok, and J. P. Dowling, J. Mod. Opt. **49**, 2325 (2002).
- [25] C. Branciard et al, Phys. Rev. A **85**, 010301(R) (2012); T. C. Ralph, Phys. Rev. A **61**, 010303(R) (1999); M. D. Reid, Phys. Rev. A **62**, 062308 (2000); *ibid.*, in *Quantum Squeezing*, editors P. D. Drummond and Z. Ficek (Springer, 2004); Ch. Silberhorn, N. Korolkova, and G. Leuchs, Phys. Rev. Lett. **88**, 167902 (2002); F. Grosshans, G. Van Assche, J. Wenger, R. Brouri, N. J. Cerf and Ph. Grangier, Nature **421**, 238 (2003).
- [26] A. Furusawa, J. L. Sorensen, S. L. Braunstein, C. A. Fuchs, H. J. Kimble, and E. S. Polzik, Science **282**, 706 (1998).
- [27] Q. Y. He, P. D. Drummond, M. K. Olsen, and M. D. Reid, Phys. Rev. A to be published, arXiv:1202.5752v1 [quant-ph].
- [28] J. Zhang, C. Xie, and K. Peng, Phys. Rev. A **66**, 042319 (2002).
- [29] W. P. Bowen, N. Treps, R. Schnabel, and P. K. Lam, Phys. Rev. Lett. **89**, 253601 (2002).
- [30] G. J. Milburn, J. Corney, E. M. Wright, and D. F. Walls, Phys. Rev. A **55**, 4318 (1997).
- [31] U. Leonhardt, Phys. Rev. A **48**, 3265 (1993).
- [32] T. J. Haigh, A. J. Ferris, and M. K. Olsen, Opt. Commun. **283**, 3540 (2010).
- [33] E. P. Wigner, Phys. Rev. **40**, 749 (1932); R. Graham, in *Springer Tracts in Modern Physics: Quantum Statistics in Optics and Solid-State Physics*, ed G. Hohler, (Springer, New York, 1973); P. D. Drummond and A. D. Hardman, Europhys. Lett. **21**, 279(1993); M. Steel, M. K. Olsen, L. I. Plimak, P. D. Drummond, S. Tan, M. J. Collett, D. Walls, and R. Graham, Phys. Rev. A, **58**, 4824 (1998); A. Sinatra, C. Lobo, and Y. Castin, J. Phys. B, **35**, 3599 (2002).
- [34] M. D. Reid and P. D. Drummond, Phys. Rev. Lett. **60**, 2731 (1988).
- [35] M. D. Reid, Phys. Rev. A **40**, 913 (1989).
- [36] L. M. Duan, G. Giedke, J. I. Cirac, and P. Zoller, Phys. Rev. Lett. **84**, 2722 (2000).
- [37] R. Simon, Phys. Rev. Lett. **84**, 2726 (2000).
- [38] V. Giovannetti, S. Mancini, D. Vitali, and P. Tombesi, Phys. Rev. A **67**, 022320 (2003).

- [39] E. G. Cavalcanti and M. D. Reid, *Journ. Mod. Opt.* **54**, 2373 (2007); E. G. Cavalcanti, P. D. Drummond, H. A. Bachor, and M. D. Reid, *Optics Express* **17**, 18693 (2009).
- [40] J. I. Cirac, M. Lewenstein, K. Molmer, and P. Zoller, *Phys. Rev. A* **57**, 1208 (1998); G. Mazzarella, L. Salasnich, A. Parola, and F. Toigo, *Phys. Rev. A* **83**, 053607 (2011); C. Bodet, J. Est'ève, M. K. Oberthaler, and T. Gasenzer, *Phys. Rev. A* **81**, 063605 (2010); J. Dunningham and K. Burnett, *Journ. Modern Optics*, **48**, 1837 (2001); D. Gordon and C. M. Savage, *Phys Rev A* **59**, 4623 (1999); L. D. Carr, D. R. Dounas-Frazer, and M. A. Garcia-March, *Europhys. Lett.* **90**, 10005 (2010); C. V. Chianca and M. K. Olsen, *Opt. Commun.* **285**, 825 (2012).
- [41] C. Lee, *Phys. Rev. Lett.* **97**, 150402 (2006); C. Lee et al, *Front. Phys.* **7**, 109 (2012); Q. Y. He, T. G. Vaughan, P. D. Drummond, and M. D. Reid arXiv:1111.5117v2 [quant-ph].
- [42] C. Gross, T. Zibold, E. Nicklas, J. Esteve, and M. K. Oberthaler, *Nature (London)* **464**, 1165 (2010).
- [43] A. Kaufman, R. Anderson, T. Hanna, E. Tiesinga, P. S. Julienne, and D. S. Hall, *Phys. Rev. A* **80**, 050701 (2009).
- [44] R. Dong, J. Heersink, J. I. Yoshikawa, O. Glockl, U. L. Andersen, and G. Leuchs, *New J. Phys.* **9**, 410 (2007).
- [45] M. Kitagawa and M. Ueda, *Phys. Rev. A* **47**, 5138 (1993).
- [46] D. J. Wineland, J. Bollinger, W. M. Itano, and D. J. Heinzen, *Phys. Rev. A* **50**, 67 (1994).
- [47] A. S. Sørensen and K. Mølmer, *Phys. Rev. Lett.* **86**, 4431 (2001).
- [48] M. F. Riedel, P. Böhi, Y. Li, T.W. Hänsch, A. Sinatra, and P. Treutlein, *Nature (London)* **464**, 1170 (2010).
- [49] M. Egorov, R. P. Anderson, V. Ivannikov, B. Opanchuk, P. Drummond, B. V. Hall, and A. I. Sidorov, *Phys. Rev. A* **84**, 021605 (2011).
- [50] H. Krauter et al, *Phys Rev Lett* **107**, 080503 (2011).
- [51] S. Chaturvedi, P. D. Drummond, and D. F. Walls, *J. Phys. A* **10**, L187 (1977).
- [52] C. V. Chianca and M. K. Olsen, to be published.
- [53] H. Risken, in *The Fokker-Planck Equation: Methods of Solution and Applications*, 2nd ed. (Springer-Verlag, Berlin, 1996).